IET Power Electronics

Research Article

IET Journals
The Institution of Engineering and Technology

Communication-free optimal economical dispatch scheme for cascaded-type microgrids with capacity constraints

ISSN 1755-4535
Received on 24th July 2019
Revised 22nd October 2019
Accepted on 12th December 2019
doi: 10.1049/iet-pel.2019.0890
www.ietdl.org

Lang Li[1], Yao Sun[1] ✉, Hua Han[1], Xiaochao Hou[1], Xufeng Yuan[2], Wei Xiong[2], Mei Su[1]

[1]*School of Automation, Central South University, Changsha 410083, People's Republic of China*
[2]*School of Electrical Engineering, Guizhou University, Guiyang 550025, People's Republic of China*
✉ *E-mail: yaosuncsu@gmail.com*

Abstract: The existing method cannot realise the optimal economical dispatch operation of cascaded-type microgrids with capacity constraints in a communication-free manner. To address this problem, a new optimal economical dispatch control scheme is proposed for the islanded cascaded-type microgrids without communications. Compared to the existing method, there are two prominent advantages: (i) global optimal economical operation with capacity constraints is realised; (ii) improved load voltage quality is obtained. Then, the stability of the proposed scheme has been analysed with a small-signal analysis method. Finally, the effectiveness of the method is verified by both simulations and experiments.

1 Introduction

Recently, interest has been concentrated on microgrids [1, 2], which is the most effective way to solve the penetration of extensively distributed generators (DGs) to power grid [3, 4]. Usually, a microgrid consists of different types of DGs that have different generation costs [5, 6]. From the perspective of economics, all DGs should be coordinated to minimise the power generation costs of microgrids.

Owing to the high reliability and communication-free features, decentralised economical operation schemes have drawn plenty of research studies [2, 7, 8]. In the microgrids, which are made up of paralleled inverters (paralleled-type microgrids), the droop control as the classical decentralised method has been widely adopted [9, 10]. The droop control strategy is initially proposed to achieve proportional power sharing by imitating the characteristic of the synchronous generator [11, 12]. However, the proportional power sharing cannot guarantee the optimised economical operation. To minimise the total active generation costs (TAGC) of paralleled-type microgrids, Nutkani *et al.* [5] introduced two linear droop control strategies, i.e. maximum and mean generation cost-based droop control. The essence of these two methods is to make the lower-cost DG hold the higher priority of output powers. However, the optimisation results might not be effective due to the non-linearity of DGs generation costs. Furthermore, Nutkani *et al.* [13] presented a non-linear cost-based droop control method. In addition, Elrayyah *et al.* [6] proposed another non-linear droop construction scheme based on the polynomial fitting method, which could lower the TAGC by selecting the proper droop coefficients. To realise the plug and play for DGs, Cingoz *et al.* [14] proposed an improved control scheme, which performs individually for each DG by optimising each one against the hypothetical DG. Then, Han *et al.* [15] proposed a curve fitting method by considering DGs capacity constraints and systems stability to realise the economical operation without communications. However, when constraints are taken into account, such as the DGs capacity constraints, it is difficult to realise the optimal economical operation without communications [15, 16].

In contrast, the cascaded-type microgrids are suited for the cases where the voltage levels are higher, and the capacity is larger [17–20]. Recently, it has been regarded as an important alternative in the medium-/high-voltage applications [21–23]. The low-voltage distributed energy resources are integrated by cascaded H-bridge inverters, then taken into the medium-/high-voltage utility grid [24, 25] or islanded power network [26, 27] by AC-stacked features. He *et al.* [26] studied the cascaded-type microgrids in the islanded mode and proposed an inverse power factor droop control for power sharing in decentralised manners. However, this strategy is unsuitable for supplying resistance–capacitance loads. Then, Sun *et al.* [27] introduced an f-P/Q droop control under the resistance–inductance and resistance–capacitance loads, which overcomes the limitations of application scope in [26]. However, both of them only deal with proportional power sharing rather than the economical operation. Li *et al.* [28] studied the economical operation of the cascaded-type microgrids and proposed a decentralised control scheme based on the fact of frequency consistency. However, two limitations exist in this method: (i) when the capacity constraints of DGs are considered, the modifications make the system deviate its optimal economical operation and obtain a sub-optimal solution; (ii) due to the different voltage phase angles of each DG, the load voltage amplitudes cannot be guaranteed strictly. Thus, a new control approach should be developed.

To address the above limitations, a new communication-free optimal economical dispatch scheme $\cos\varphi - f/P - V$ is proposed. The power factors of each DG are regulated to the same value, and the output voltage amplitudes are used to allot the output power of each DG. As long as the optimal solution of the formulated economical optimisation problem could be solved, the proposed method can achieve the optimal economical dispatch operation of the cascaded-type microgrids without communications. Compared to the existing method [28], the proposed scheme has two obvious advantages:

- *Global optimal economical operation:* The method proposed in [28] is a sub-optimal economical operation due to the modifications. In this work, the global optimal economical operation with capacity constraints is realised without communications.
- *Improved load voltage quality*: The load voltage amplitudes cannot be guaranteed strictly with the method proposed in [28]. On the contrary, the proposed scheme can control the load voltage amplitudes to maintain the desired values. Also, the excellent load voltage quality is obtained.

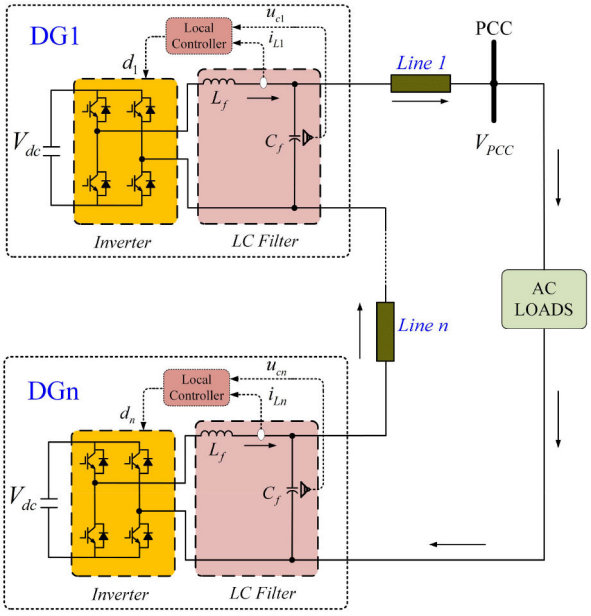

Fig. 1 *Cascaded-type microgrids*

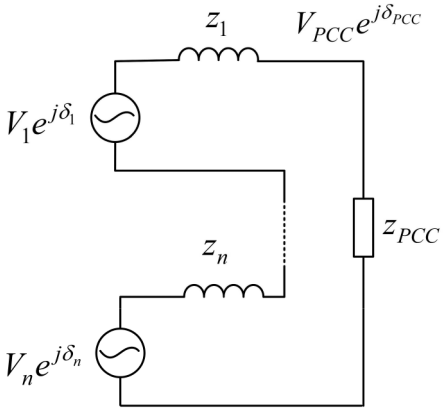

Fig. 2 *Equivalent circuit of cascaded-type microgrids*

2 Economical optimisation of cascaded-type microgrids

2.1 Cascaded-type microgrids

Fig. 1 presents the structure of islanded cascaded-type microgrids, which comprises n cascaded micro-inverters. Then, the equivalent circuit is shown in Fig. 2. In Figs. 1 and 2, $\boldsymbol{V}_i\mathrm{e}^{\mathrm{j}\delta_i}$ presents the output voltage vector of the ith DG, $\boldsymbol{V}_{\mathrm{PCC}}\mathrm{e}^{\mathrm{j}\delta_{\mathrm{PCC}}}$ is the voltage vector at the PCC. V_i and V_{PCC} denote the corresponding voltage amplitudes, δ_i and δ_{PCC} are the corresponding voltage phase angles. L_{f} and C_{f} express the filter inductance and filter capacitance, respectively. R_{f} and R_{d} are the corresponding series resistances. z_{PCC} is the load impedance and z_i denotes the line impedance.

According to Kirchhoff laws, $\boldsymbol{V}_{\mathrm{PCC}}\mathrm{e}^{\mathrm{j}\delta_{\mathrm{PCC}}}$ is expressed as

$$\boldsymbol{V}_{\mathrm{PCC}}\mathrm{e}^{\mathrm{j}\delta_{\mathrm{PCC}}} = y'z_{\mathrm{PCC}}\sum_{i=1}^{n}V_i\mathrm{e}^{\mathrm{j}\delta_i} \tag{1}$$

$$y' = 1/\left(z_{\mathrm{PCC}} + \sum_{i=1}^{n}z_i\right) \tag{2}$$

where y' is the equivalent admittance. For simplification, y' is rewritten as

$$y' = |Y'|\mathrm{e}^{\mathrm{j}\theta'} \tag{3}$$

where $|Y'|$ and θ' denote its corresponding modulus and phase angle of y'. Then, the instantaneous active power p_i and reactive power q_i are written as

$$p_i = V_i|Y'|\sum_{j=1}^{n}V_j\cos(\delta_i - \delta_j - \theta') \tag{4}$$

$$q_i = V_i|Y'|\sum_{j=1}^{n}V_j\sin(\delta_i - \delta_j - \theta') \tag{5}$$

After passing a first-order low-pass filter, the filtered active power P_i and reactive power Q_i are expressed as

$$\dot{P}_i = \omega_{\mathrm{c}}p_i - \omega_{\mathrm{c}}P_i \tag{6}$$

$$\dot{Q}_i = \omega_{\mathrm{c}}q_i - \omega_{\mathrm{c}}Q_i \tag{7}$$

where ω_{c} is the cut-off frequency of the low-pass filter.

From (4)–(7), it can be concluded that P_i and Q_i are controlled by regulating the amplitude differences and phase-angle differences of DGs output voltages.

2.2 Economical optimisation problem formulation

Usually, the economical optimisation problem of power systems could be formulated as

$$\begin{aligned}&\min\left(\sum C_i(P_i)\right)\\ &\text{s.t.}\quad \sum P_i = P_{\mathrm{L}}\\ &P_{i,\min} \le P_i \le P_{i,\max}\end{aligned} \tag{8}$$

where P_{L} are the active power load demands including the transmission line losses. The subscripts 'max' and 'min' indicate the corresponding maximum and minimum values. $P_{i,\min}$, $P_{i,\max}$ are the allowed output active power of the ith DG. $C_i(P_i)$ is the general comprehensive operational costs consisting of fuel costs, maintenance costs, and so on, $i \in \{1, 2, \ldots, n\}$.

Assume that $C_i(P_i)$ is continuous, it follows from the extreme value theorem such that the economical optimisation problem has a globally optimal solution $(P_1^*, P_2^*, \ldots, P_n^*)$ [29]. Also, the optimal solution P_i^* is a map of P_{L}, which is expressed as

$$P_i^* = g_i(P_{\mathrm{L}}) \tag{9}$$

where $g_i(P_{\mathrm{L}})$ is the optimal economical operation function (OEOF) of P_{L}. Usually, $g_i(P_{\mathrm{L}})$ can be obtained by off-line calculation in advance. It is worth noting that the focus of this study is not about how to solve the optimal solution but how to design a controller only based on the local information to realise the optimal economical operation of the studied system.

3 Proposed communication-free economical operation control scheme

To implement the optimal solution formula (9) and maintain the desired load voltage amplitudes, the proposed communication-free $\cos\varphi - f/P - V$ control is introduced in this section.

3.1 Proposed control scheme

The proposed $\cos\varphi - f/P - V$ control scheme of the ith DG in the cascaded-type microgrids is expressed as

$$f_i = f^* + m\mathrm{sgn}(Q_i)\cos\varphi_i \tag{10}$$

$$V_i = \frac{g_i(\bar{P}_i)}{\sum_{j=1}^{n}g_j(\bar{P}_i)}V_{\mathrm{PCC}}^* \tag{11}$$

where

$$\bar{P}_i = V^*_{\mathrm{PCC}} I_i \cos\varphi_i \tag{12}$$

$$\cos\varphi_i = \frac{P_i}{\sqrt{P_i^2 + Q_i^2}} \tag{13}$$

where f^* is the nominal frequency of the microgrids, f_i is the reference frequency of the ith DG. φ_i is the power factor angle of the ith DG. V^*_{PCC} is the reference voltage at PCC. $\mathrm{sgn}(\cdot)$ is a signum function. m is a certain positive coefficient determined by the feasible frequency ranges $[f_{\min}, f_{\max}]$. $f_{\max}$ and $f_{\min}$ are the given maximum and minimum permissible frequency. Usually, the nominal frequency takes the value of $(f_{\max} + f_{\min})/2$. According to (10), m should be designed to satisfy the constraint: $0 < m \leq (f_{\max} - f_{\min})/2$.

3.2 Steady-state analysis

In the steady state, the following equality for two different DGs is obtained from (10)

$$\cos\varphi_i = \cos\varphi_j \tag{14}$$

Equation (14) means that those power factors of each DG in the microgrids are the same under the proposed scheme.

Remark 1: Keeping the same power factor is very crucial because it ensures: (i) the power sharing is proportional to its output voltage amplitudes; (ii) the same voltage phase of each DG to add them algebraically; (iii) acquiring the load information locally.

Since all the DGs have the same power factor, combine $I_i = I_j$ and $P_i = V_i I_i \cos\varphi_i$, then the following equalities hold:

$$P_i : P_j = V_i : V_j \tag{15}$$

$$\bar{P}_i = \bar{P}_j \tag{16}$$

Clearly, the active power allocations depend on the choice of the output voltage amplitudes shown in Fig. 3, in which ω_{s} is the synchronous frequency of the cascaded-type microgrids in the steady state.

Remark 2: The output power of each DG is proportional to its output voltage amplitudes, which is the foundation of economical allocation. We could regulate the voltage reference to realise the economical operation, which is totally different from the idea in [28].

Substituting (11) into (15), and combining (16), we have

$$P_i : P_j = g_i(\bar{P}_i) : g_j(\bar{P}_j) \tag{17}$$

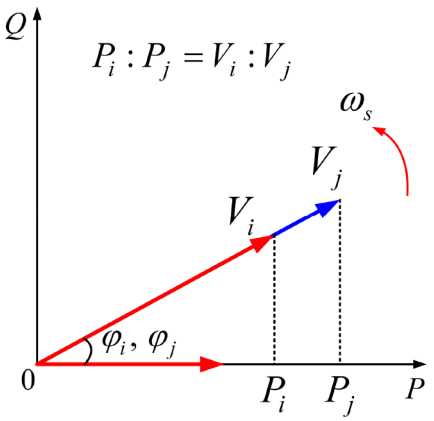

Fig. 3 *Power operation control of the proposed scheme*

In fact, according to the definition of $\bar{P}_i$ in (12), $\bar{P}_i$ in the steady state is equal to P_{L}, which can be obtained only based on the local measurements. Thus, (17) is rewritten as follows:

$$P_i : P_j = g_i(P_{\mathrm{L}}) : g_j(P_{\mathrm{L}}) \tag{18}$$

Combining (18) with (9), yields

$$P_i : P_j = P_i^* : P_j^* \tag{19}$$

Since $\sum P_i = \sum P_i^* = P_{\mathrm{L}}$, then we have

$$P_i = P_i^* \tag{20}$$

Remark 3: From (20), the output power of each DG under schemes (10) and (11) is the optimal solution of problem (8). That is to say, the first limitation in [28] is solved. From (10) and (11), the control scheme only depends on each DG's output voltage and current, so $\cos\varphi - f/P - V$ is a communication-free control approach.

Usually, the feeder impedance is much less than the load impedance. Consequently, the voltage drop on feeder impedance can be neglected. Since the same voltage phase of each DG is achieved according to (10), then, $\left|\sum V_i \mathrm{e}^{\mathrm{j}\delta_i}\right| = V^*_{\mathrm{PCC}}$. Thus, the expected load voltage amplitudes are obtained while satisfying the optimality. Also, the second limitation in [28] is overcome.

Overall, it can be summarised as follows: the proposed scheme can perform the optimal solution via the decentralised manner while satisfying the desired load voltage amplitudes.

4 Stability analysis

As the economical operation is closely related to the underlying control of the microgrids, the stability of systems with consideration of economical operation is a critical issue. Thus, the stability and sensibility analysis of parameters will be investigated in this section through the small-signal analysis method [30–32].

Equation (10) is rewritten as

$$\omega_i = \omega^* + 2\pi m \mathrm{sgn}(Q_i)\cos\varphi_i \tag{21}$$

where $\omega^* = 2\pi f^*$. Let $\delta_{\mathrm{s}} = \int \omega_{\mathrm{s}}\,\mathrm{d}t$, and denote $\tilde{\delta}_i = \delta_i - \delta_{\mathrm{s}}$, then we have

$$\dot{\tilde{\delta}}_i = \omega^* - \omega_{\mathrm{s}} + 2\pi m \mathrm{sgn}(Q_i)\cos\varphi_i \tag{22}$$

Linearisation of (6) and (7) yields

$$\begin{aligned}\Delta\dot{P}_i = {} & \omega_{\mathrm{c}}\frac{\partial p_i}{\partial V_i}\Delta V_i + \omega_{\mathrm{c}}\sum_{j=1,i\neq j}^{n}\frac{\partial p_i}{\partial V_j}\Delta V_j \\ & + \omega_{\mathrm{c}}\frac{\partial p_i}{\partial \tilde{\delta}_i}\Delta\tilde{\delta}_i + \sum_{j=1,i\neq j}^{n}\frac{\partial p_i}{\partial \tilde{\delta}_j}\Delta\tilde{\delta}_j - \omega_{\mathrm{c}}\Delta P_i\end{aligned} \tag{23}$$

$$\begin{aligned}\Delta\dot{Q}_i = {} & \omega_{\mathrm{c}}\frac{\partial q_i}{\partial V_i}\Delta V_i + \omega_{\mathrm{c}}\sum_{j=1,i\neq j}^{n}\frac{\partial q_i}{\partial V_j}\Delta V_j \\ & + \omega_{\mathrm{c}}\frac{\partial q_i}{\partial \tilde{\delta}_i}\Delta\tilde{\delta}_i + \sum_{j=1,i\neq j}^{n}\frac{\partial q_i}{\partial \tilde{\delta}_j}\Delta\tilde{\delta}_j - \omega_{\mathrm{c}}\Delta Q_i\end{aligned} \tag{24}$$

Combining $I_i = \sqrt{P_i^2 + Q_i^2}/V_i$ with (13), (12) is rewritten as

$$\bar{P}_i = V^*_{\mathrm{PCC}} P_i / V_i \tag{25}$$

By substituting (25) into (11), then it is rewritten as

$$F_i(V_i, P_i) = 0 \tag{26}$$

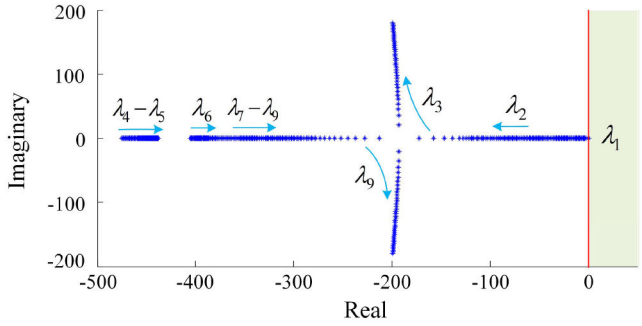

Fig. 4 *Root locus as m increases from 0.01 to 0.5*

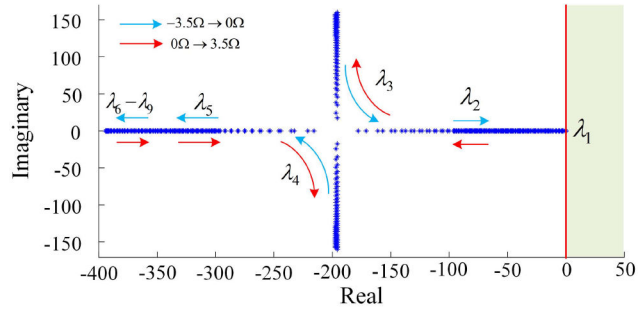

Fig. 5 *Root locus as* $X_{load} \in [-3.5,\ 3.5]$

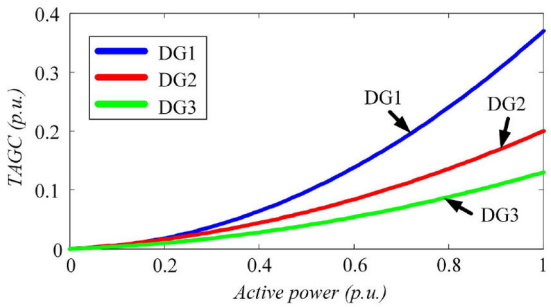

Fig. 6 *TAGC of DG1, DG2, and DG3*

where $F_i(\cdot)$ is the function of V_i and P_i. Linearisation of (26) yields

$$\Delta V_i = a_i \Delta P_i \tag{27}$$

where $a_i = -((\partial F_i/\partial P_i)/(\partial F_i/\partial V_i))$. Combining (22)–(24) and (27), the small signal model of the ith DG is

$$\Delta\dot{\tilde{\delta}}_i = -2\pi m \mathrm{sgn}(Q_i^o)\sin\varphi_i^o\left(\frac{\partial\varphi_i}{\partial P_i}\Delta P_i + \frac{\partial\varphi_i}{\partial Q_i}\Delta Q_i\right) \tag{28}$$

$$\begin{aligned}\Delta\dot{P}_i = {} & \omega_c\left(\frac{\partial p_i}{\partial V_i}a_i - 1\right)\Delta P_i + \omega_c\sum_{j=1,i\neq j}^{n}\frac{\partial p_i}{\partial V_j}a_j\Delta P_j \\ & + \omega_c\frac{\partial p_i}{\partial\tilde{\delta}_i}\Delta\tilde{\delta}_i + \omega_c\sum_{j=1,i\neq j}^{n}\frac{\partial p_i}{\partial\tilde{\delta}_j}\Delta\tilde{\delta}_j\end{aligned} \tag{29}$$

$$\begin{aligned}\Delta\dot{Q}_i = {} & \omega_c\frac{\partial q_i}{\partial V_i}a_i\Delta P_i + \omega_c\sum_{j=1,i\neq j}^{n}\frac{\partial q_i}{\partial V_j}a_j\Delta P_j \\ & + \omega_c\frac{\partial q_i}{\partial\tilde{\delta}_i}\Delta\tilde{\delta}_i + \omega_c\sum_{j=1,i\neq j}^{n}\frac{\partial q_i}{\partial\tilde{\delta}_j}\Delta\tilde{\delta}_j - \omega_c\Delta Q_i\end{aligned} \tag{30}$$

Write (28)–(30) in the matrix form

$$\dot{\boldsymbol{X}} = \boldsymbol{A}\boldsymbol{X} \tag{31}$$

Table 1 Parameters for simulations

Parameters	Values	Parameters	Values
f, Hz	[49, 51]	R_d, Ω	3.3
f^*, Hz	50	L_{Line1}, H	1.5×10^{-3}
m	0.3	L_{Line2}, H	1.6×10^{-3}
V^*_{PCC}, V	110	L_{Line3}, H	1.2×10^{-3}
L_f, H	1.5×10^{-3}	P_{max}, W	1000
R_f, Ω	0.4	Q_{max}, Var	1000
C_f, μF	20	P_i, p.u.	[0, 1]

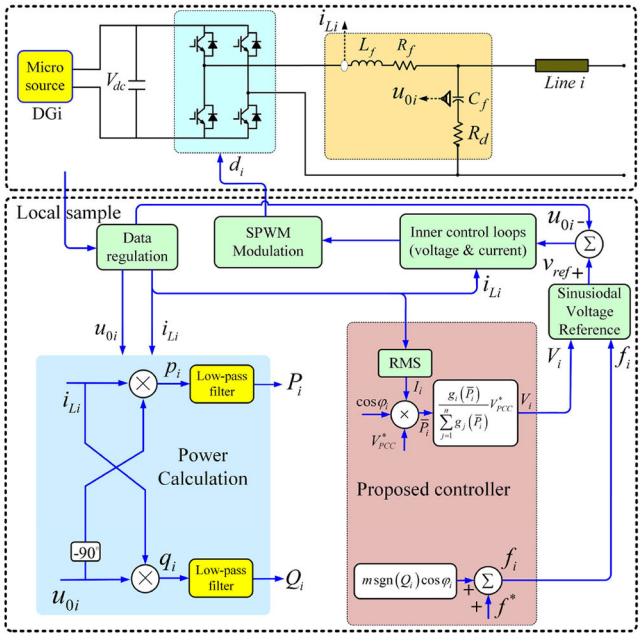

Fig. 7 *Control block diagram of the single-phase DG unit*

where $\boldsymbol{X}$ is the state variable vector and $\boldsymbol{A}$ is the system matrix. Both of them are shown in the Appendix. The root locus method is used to investigate the system stability around the operating point. Based on the simulation system described in Section 5, the root locus diagrams under different m and the load reactance X_{load} are studied.

Fig. 4 shows the root locus diagram as m increases from 0.01 to 0.5, with the load resistance $R_{load} = 12.5\,\Omega$, $X_{load} = 3.14\,\Omega$. As seen, matrix $\boldsymbol{A}$ has one zero eigenvalue as to rotational invariance, which is depicted in [33]. The rest eigenvalues are in the left half-plane. As seen, the system is stable when $m \in [0.01, 0.5]$.

When $R_{load} = 12.5\,\Omega$, $m = 0.3$, then let X_{load} changes from $-3.5\,\Omega$ to $3.5\,\Omega$, the root locus diagram is depicted in Fig. 5. As seen, the proposed scheme can maintain the system stable operation under both the resistance–capacitance loads and resistance–inductance loads.

5 Simulation results

The proposed $\cos\varphi - f/P - V$ scheme is verified in the MATLAB/Simulink platform. The cascaded-type microgrid in the simulation model includes three DGs (see Fig. 1). The generation costs of DGs from the literature [5, 15] are depicted in Fig. 6. The parameters of the simulation are listed in Table 1. The detailed control block diagram of the DG unit is shown in Fig. 7.

5.1 Case 1: switch between the resistance–inductance and resistance–capacitance load

This simulation is carried out under both the resistance–inductance and resistance–capacitance loads. The load demands are scheduled as follows: in the interval [0 s, 1 s] resistance–capacitance load, in [1 s, 2 s] resistance–inductance load, and resistance–capacitance

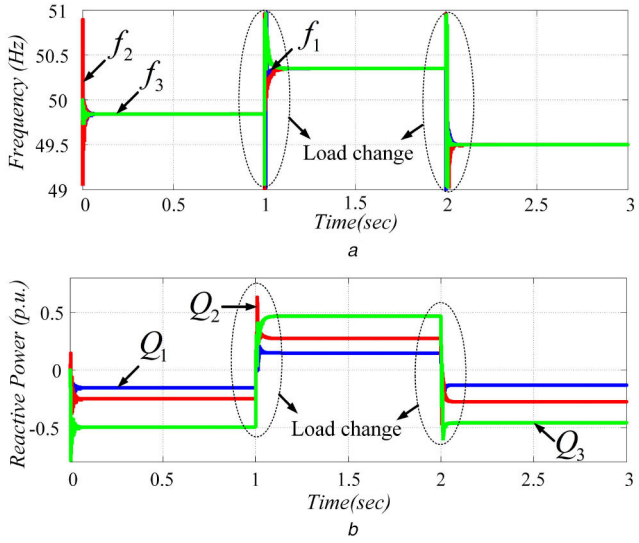

Fig. 8 *Simulation results of case 1*

(a) Frequency, ***(b)*** Reactive power under the resistance–inductance and resistance–capacitance load

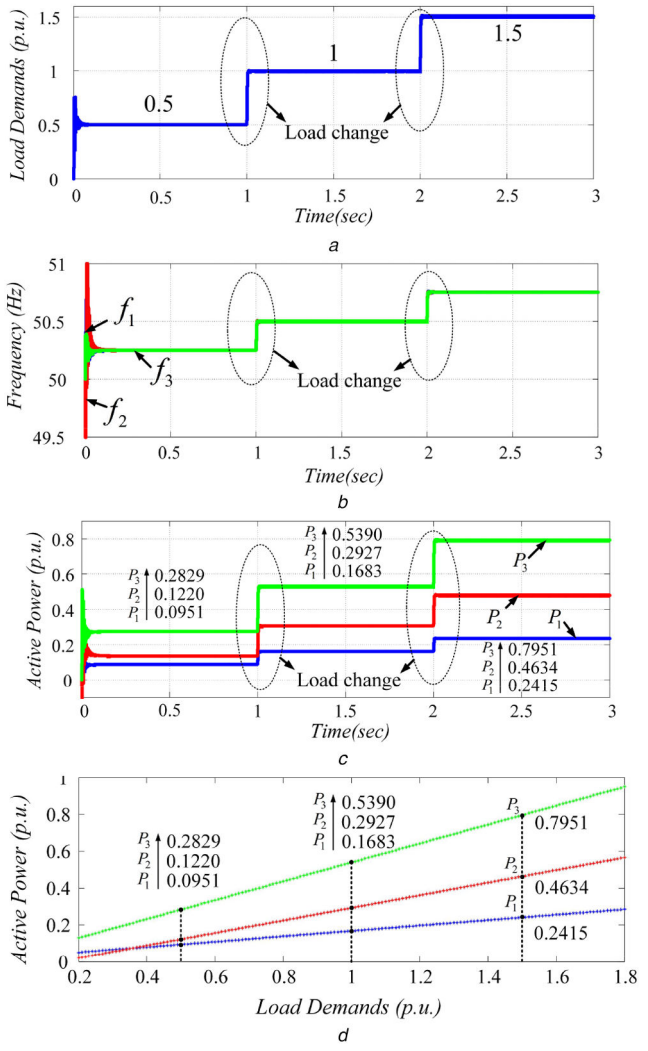

Fig. 9 *Simulation results of case 2*

(a) Active power load demands, ***(b)*** Frequency, ***(c)*** Active power allocations, ***(d)*** OEOF

load in the interval [2 s, 3 s]. The frequencies over time are depicted in Fig. 8*a*.

The reactive power allocations among DGs are shown in Fig. 8*b*. Therefore, the proposed scheme can realise the stable operation under the two types of load.

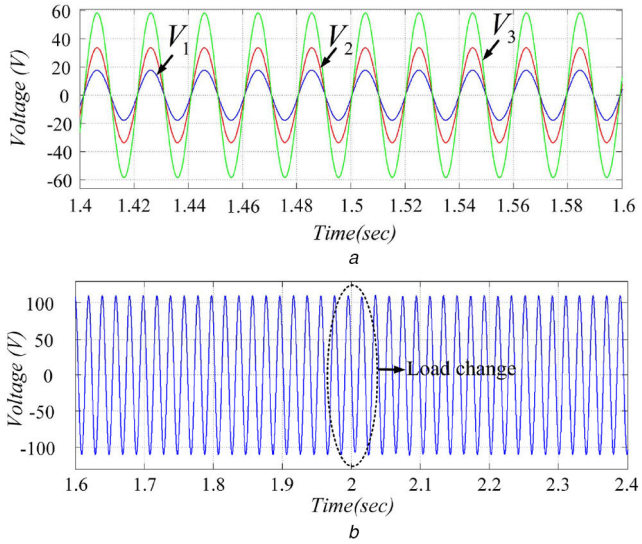

Fig. 10 *Simulation voltage waveforms*

(a) DGs in the steady state, ***(b)*** PCC during load changing

5.2 Case 2: optimal economical operation under resistance–inductance load

To verify the optimal economical operation under the resistance–inductance load, the load demands shown in Fig. 9*a* are scheduled as 0.5, 1 and 1.5 p.u. in the interval [0 s, 1 s], [1 s, 2 s] and [2 s, 3 s], respectively. The frequencies are shown in Fig. 9*b*, which is >50 Hz due to the feature of inverse droop. The active power sharing results are shown in Fig. 9*c*. The OEOF solved by the interior point method [34] is depicted in Fig. 9*d*. Clearly, the operation results in Fig. 9*c* agree with Fig. 9*d*. It is concluded that the proposed scheme can obtain the optimal economical operation under the resistance–inductance load.

Fig. 10*a* shows the voltage waveform of each DG in the interval [1.4 s, 1.6 s]. The voltage phase angles of DGs are controlled to be the same value, but the voltage amplitudes are different. The load voltage at PCC is shown in Fig. 10*b*, in which its amplitudes keep 110 V regardless of the load changes. Therefore, the proposed scheme can obtain an excellent load voltage quality.

5.3 Case 3: optimal economical operation under resistance–capacitance load

This simulation is carried out to verify the performance of the proposed scheme under the resistance–capacitance load. The active power load schedules are the same as case 2 (see Fig. 9*a*). The waveform of frequencies is shown in Fig. 11*a*. It is <50 Hz because the droop control is performed. The active power allocations among DGs are shown in Fig. 11*b*, which agree with Fig. 9*d*. Therefore, the optimal economical operation is also obtained under the resistance–capacitance load.

5.4 Case 4: capacity constrains

As shown in Fig. 12*a*, the load demands are scheduled as 1.8, 2 and 2.2 p.u. in the interval [0 s, 1 s], [1 s, 2 s] and [2 s, 3 s], respectively. The frequencies are depicted in Fig. 12*b*. The active power allocations among DGs are shown in Fig. 12*c*, in which P_3 keeps its maximum output power (1 p.u.) in the second and third intervals. The OEOF curve is depicted in Fig. 12*d* with $P_{\mathrm{L}} \in [1.6\,\mathrm{p.u.}, 2.4\,\mathrm{p.u.}]$. Obviously, the simulation results in Fig. 12*c* agree with the theoretical results in Fig. 12*d*. Thus, the proposed scheme is capable of capacity constrains for DGs.

5.5 Case 5: comparisons between the proposed scheme and the method in [28]

In this case, the load demands are set as 2 and 2.2 p.u. in the intervals [0 s, 1 s] and [1 s, 2 s], respectively. From the comparative results shown in Fig. 13*a*, the TAGC of the proposed

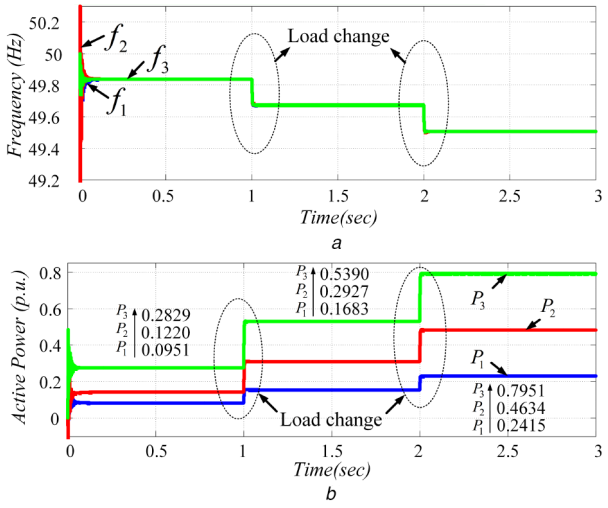

Fig. 11 *Simulation results of case 3*
(a) Frequency, ***(b)*** Active power allocations

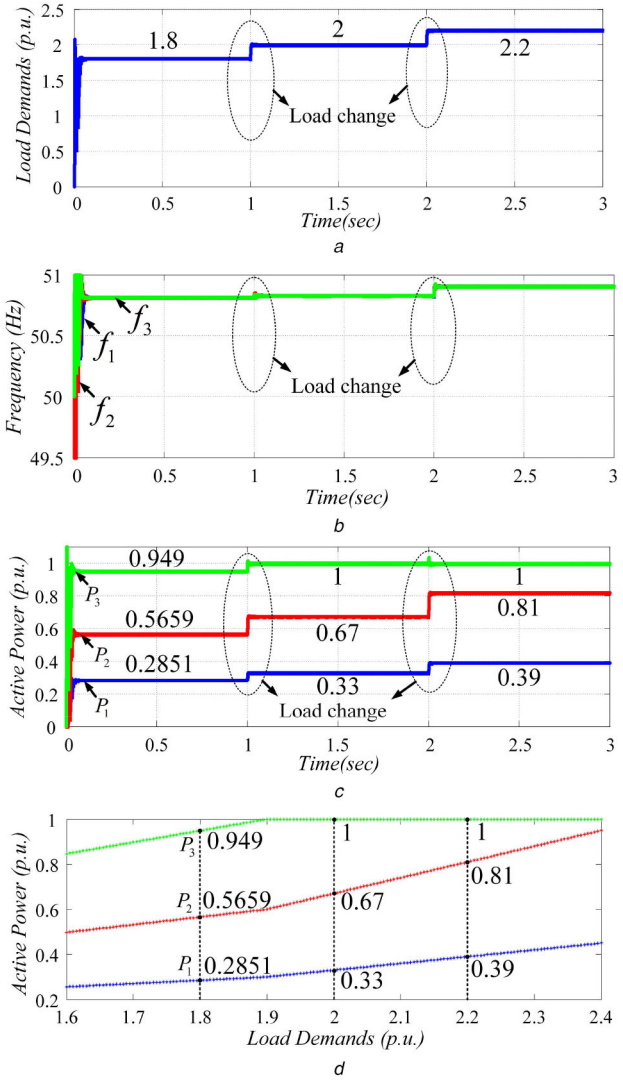

Fig. 12 *Simulation results of case 4*
(a) Active power load demands, ***(b)*** Frequency, ***(c)*** Active power allocations, ***(d)*** OEOF

scheme is lower than that based on the method proposed in [28]. Therefore, the proposed scheme is preferable to the method proposed in [28] from the perspective of the economy. The load voltage amplitudes are shown in Fig. 13*b*, in which the proposed scheme can maintain the desired values. On the contrary, the load voltage amplitudes of the method in [28] deviate from its nominal

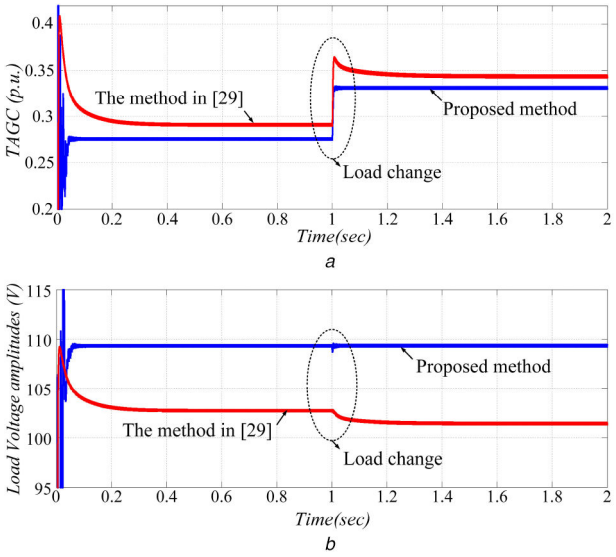

Fig. 13 *Comparison results*
(a) TAGC, ***(b)*** Load voltage amplitudes

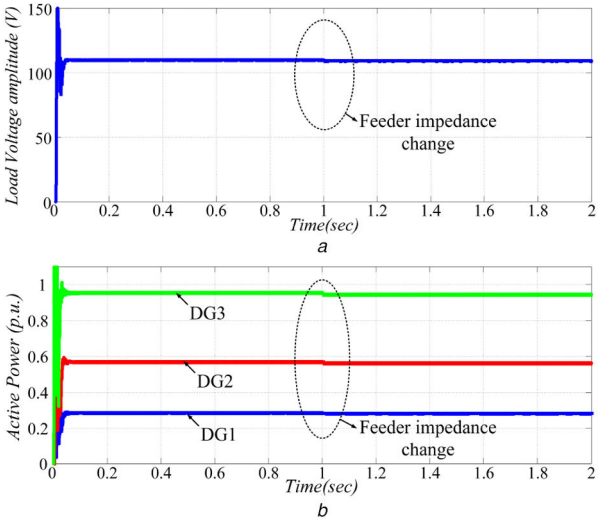

Fig. 14 *Simulation results of case 6*
(a) Load voltage amplitudes, ***(b)*** Active power allocations

values. As seen, the proposed scheme is superior to the method [28] in the point of economy and load voltage quality.

5.6 Case 6: performance of the proposed scheme under the feeder impedance variation

This test with feeder impedance variation (from 1.5 to 3 mH) at $t =$ 1 s is performed. The load voltage amplitudes are shown in Fig. 14*a*, which almost maintains a constant level. The active power allocations are depicted in Fig. 14*b*, which also almost maintains a constant. Therefore, the effect of feeder impedance variation on the performance of the proposed method is almost negligible. That is to say, the proposed scheme is robust to the feeder impedance variation to some extent.

6 Experimental results

In order to verify the performance of the proposed $\cos\varphi - f/P - V$ scheme, a microgrid prototype is built shown in Fig. 15 including two DGs, which are simulated by a single phase voltage source inverter controlled by digital signal processor TMS320f28335. The corresponding generation costs of the two DGs are the same as those of DG1 and DG2 in the simulation models, respectively. The parameters of this experiment are listed in Table 2.

The considered microgrid comprises two DGs. Even though, it could still meet the experimental requirements. The experiment is

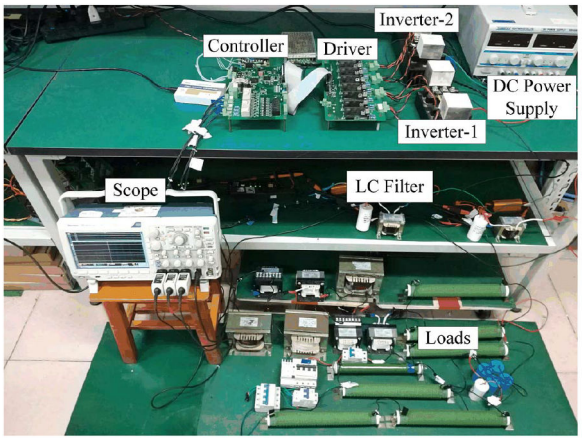

Fig. 15 *Prototype setup of the cascaded-type microgrid with two DGs*

Table 2 Parameters for experiments

Parameters	Values	Parameters	Values
f^*, Hz	50	R_d, Ω	5
m	0.3	L_{Line1}, H	0.3×10^{-3}
V^*_{PCC}, V	100	L_{Line2}, H	1.6×10^{-3}
L_f, H	0.6×10^{-3}	P_{max}, W	200
R_f, Ω	0.5	Q_{max}, Var	200
C_f, μF	20	P_i, p.u.	[0, 1]

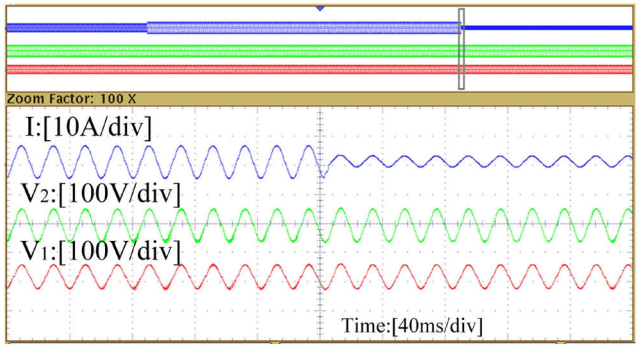

Fig. 16 *Experimental waveforms with load stepping*

implemented under the resistance–inductance load. The active power load schedules are 0.4, 0.8, 1.2, 0.4 and 0.8 p.u. in the interval [0 s, 20 s], [20 s, 40 s], [40 s, 60 s], [60 s, 80 s] and [80 s, 100 s], respectively. The experimental waveforms of voltage and current are shown in Fig. 16, in which the voltage phase angles of DG1 and DG2 are always in phase. Therefore, the proposed scheme can ensure the synchronous operation of DGs and maintain the stability of the system.

The active power requirement curve of the load is shown in Fig. 17*a*. The frequency curve is shown in Fig. 17*b*. The active power allocations among DG1 and DG2 are depicted in Fig. 17*c*. The OEOF curves are depicted in Fig. 17*d* in the case of $P_L \in [0.1\,\text{p.u.}, 1.4\,\text{p.u.}]$. Compared to Fig. 17*d*, the experimental results in Fig. 17*c* match the theoretical value approximately. The deviation of output power between Fig. 17*c* and *d* is because of the line losses. As seen, the proposed scheme can obtain the optimal economical operation without communications.

7 Conclusion

The optimal economical operation problem of the cascaded-type microgrids is studied. A communication-free control scheme (cos $\varphi - f/P - V$) is proposed, which could achieve the global optimal economical operation easily. With this method, the excellent load voltage quality is guaranteed, and its implementation only needs the local information. Meanwhile, the synchronisation of all DGs

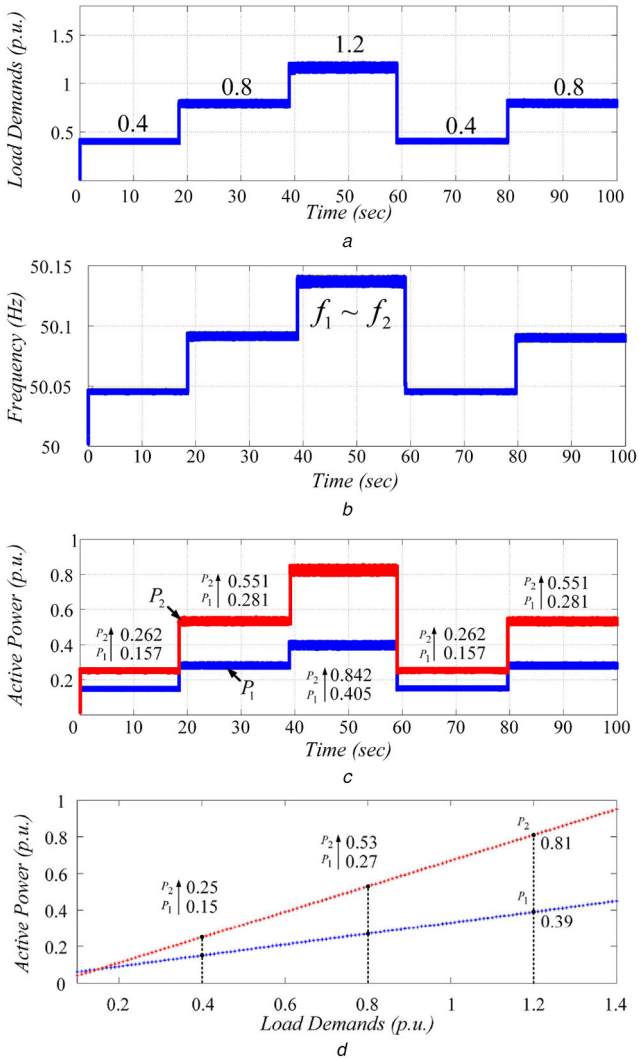

Fig. 17 *Experimental results*

(a) Active power load demands, ***(b)*** Frequency, ***(c)*** Active power allocations, ***(d)*** OEOF

has been achieved autonomously under both the inductive and capacitive loads. Besides, the large-signal stability for the system suffering large disturbance such as short-circuit faults will be investigated in the future.

8 References

[1] Peng, Z., Wang, J., Wen, Y., *et al.*: 'Virtual synchronous generator control strategy incorporating improved governor control and coupling compensation for AC microgrid', *IET Power Electron.*, 2019, **12**, (6), pp. 1455–1461

[2] Jie, Y., Xinmin, J., Xuezhi, W., *et al.*: 'Decentralised control method for DC microgrids with improved current sharing accuracy', *IET Gener. Transm. Distrib.*, 2017, **11**, (3), pp. 696–706

Q3 [3] Sun, Y., Hou, X., Yang, J., *et al.*: 'New perspectives on droop control in AC microgrid', *IEEE Trans. Ind. Electron.*, 2017, **64**, (7), pp. 5741–5745

[4] Sun, X., Liu, B., Cai, Y., *et al.*: 'Frequency-based power management for photovoltaic/battery/fuel cell-electrolyser stand-alone microgrid', *IET Power Electron.*, 2016, **9**, (13), pp. 2602–2610

[5] Nutkani, I.U., Loh, P.C., Wang, P., *et al.*: 'Linear decentralized power sharing schemes for economic operation of AC microgrids', *IEEE Trans. Ind. Electron.*, 2016, **63**, (1), pp. 225–234

[6] Elrayyah, A., Cingoz, F., Sozer, Y.: 'Construction of nonlinear droop relations to optimize islanded microgrid operation', *IEEE Trans. Ind. Appl.*, 2015, **51**, (4), pp. 3404–3413

[7] Augustine, S., Lakshminarasamma, N., Mishra, M.K.: 'Control of photovoltaic-based low-voltage dc microgrid system for power sharing with modified droop algorithm', *IET Power Electron.*, 2016, **9**, (6), pp. 1132–1143

[8] Olivares, D.E., Mehrizi-Sani, A., Etemadi, A.H., *et al.*: 'Trends in microgrid control', *IEEE Trans. Smart Grid*, 2014, **5**, (4), pp. 1905–1919

[9] Maulik, A., Das, D.: 'Optimal operation of droop-controlled islanded microgrids', *IEEE Trans. Sustain. Energy*, 2018, **9**, (3), pp. 1337–1348

[10] Guan, Y., Guerrero, J.M., Zhao, X., *et al.*: 'A new way of controlling parallel-connected inverters by using synchronous-reference-frame virtual impedance loop – part I: control principle', *IEEE Trans. Power Electron.*, 2016, **31**, (6), pp. 4576–4593

[11] Yu, M., Huang, W., Tai, N., *et al.*: 'Transient stability mechanism of grid-connected inverter-interfaced distributed generators using droop control strategy', *Appl. Energy*, 2018, **210**, pp. 737–747

[12] Lee, C.T.: 'A new droop control method for the autonomous operation of distributed energy resource interface converters', *IEEE Trans. Power Electron.*, 2013, **28**, (4), pp. 1980–1993

[13] Nutkani, I.U., Loh, P.C., Blaabjerg, F.: 'Droop scheme with consideration of operating costs', *IEEE Trans. Power Electron.*, 2014, **29**, (3), pp. 1047–1052

[14] Cingoz, F., Elrayyah, A., Sozer, Y.: 'Plug-and-play nonlinear droop construction scheme to optimize islanded microgrid operations', *IEEE Trans. Power Electron.*, 2017, **32**, (4), pp. 2743–2756

[15] Han, H., Li, L., Wang, L., *et al.*: 'A novel decentralized economic operation in islanded AC microgrids', *Energies*, 2017, **10**, (6), pp. 1–18

[16] Liu, Z., Su, M., Sun, Y., *et al.*: 'Optimal criterion and global/sub-optimal control schemes of decentralized economical dispatch for AC microgrid', *Int. J. Electr. Power Energy Syst.*, 2019, **104**, pp. 38–42

[17] Mortezaei, A., Simões, M.G., Busarello, T.D.C., *et al.*: 'Grid-connected symmetrical cascaded multilevel converter for power quality improvement', *IEEE Trans. Ind. Appl.*, 2018, **54**, (3), pp. 2792–2805

[18] Qi, C., Chen, X., Su, L., *et al.*: 'Two-voltage hierarchical model predictive control for a single-phase cascaded H-bridge rectifier', *IET Power Electron.*, 2019, **12**, (7), pp. 1634–1642

[19] Malinowski, M., Gopakumar, K., Rodriguez, J., *et al.*: 'A survey on cascaded multilevel inverters', *IEEE Trans. Ind. Electron.*, 2010, **57**, (7), pp. 2197–2206

[20] Karasani, R.R., Borghate, V.B., Meshram, P.M., *et al.*: 'A three-phase hybrid cascaded modular multilevel inverter for renewable energy environment', *IEEE Trans. Power Electron.*, 2017, **32**, (2), pp. 1070–1087

[21] Yu, Y., Konstantinou, G., Hredzak, B., *et al.*: 'Power balance of cascaded H-bridge multilevel converters for large-scale photovoltaic integration', *IEEE Trans. Power Electron.*, 2016, **31**, (1), pp. 292–303

[22] Zhang, L., Sun, K., Xing, Y., *et al.*: 'A modular grid-connected photovoltaic generation system based on DC bus', *IEEE Trans. Power Electron.*, 2011, **26**, (2), pp. 523–531

[23] Li, L., Sun, Y., Han, H., *et al.*: 'A decentralized control for cascaded inverters in grid-connected applications', *IEEE Trans. Ind. Electron.*, Early access, https://doi.org/10.1109/TIE.2019.2945266

Q4 [24] Chatzinikolaou, E., Rogers, D.J.: 'A comparison of grid-connected battery energy storage system designs', *IEEE Trans. Power Electron.*, 2017, **32**, (9), pp. 6913–6923

[25] He, J., Li, Y., Wang, C., *et al.*: 'Hybrid microgrid with parallel- and series-connected microconverters', *IEEE Trans. Power Electron.*, 2018, **33**, (6), pp. 4817–4831

[26] He, J., Li, Y., Liang, B., *et al.*: 'Inverse power factor droop control for decentralized power sharing in series-connected-microconverters-based islanding microgrids', *IEEE Trans. Ind. Electron.*, 2017, **64**, (9), pp. 7444–7454

[27] Sun, Y., Shi, G., Li, X., *et al.*: 'An f-P/Q droop control in cascaded-type microgrid', *IEEE Trans. Power Syst.*, 2018, **33**, (1), pp. 1136–1138

[28] Li, L., Ye, H., Sun, Y., *et al.*: 'A communication-free economical-sharing scheme for cascaded-type microgrids', *Int. J. Electr. Power Energy Syst.*, 2019, **104**, pp. 1–9

[29] Guo, F., Wen, C., Mao, J., *et al.*: 'Distributed economic dispatch for smart grids with random wind power', *IEEE Trans. Smart Grid*, 2016, **7**, (3), pp. 1572–1583

[30] Pogaku, N., Prodanovic, M., Green, T.: 'Modeling, analysis and testing of autonomous operation of an inverter-based microgrid', *IEEE Trans. Power Electron.*, 2007, **22**, (2), pp. 613–625

[31] Mohamed, Y.A.-R.I., El-Saadany, E.F.: 'Adaptive decentralized droop controller to preserve power sharing stability of paralleled inverters in distributed generation microgrid', *IEEE Trans. Power Electron.*, 2008, **23**, (6), pp. 2806–2816

[32] Guo, X.Q., Lu, Z.G., Wang, B.C., *et al.*: 'Dynamic phasors-based modeling and stability analysis of droop-controlled inverters for microgrid applications', *IEEE Trans. Smart Grid*, 2014, **5**, (6), pp. 2980–2987

[33] Simpson-Porco, J.W., Dörfler, F., Bullo, F.: 'Synchronization and power sharing for droop-controlled inverters in islanded microgrids', *Automatica*, 2013, **49**, (9), pp. 2603–2611

[34] Byrne, C.L.: 'Iterative optimization', '*A First Course in Optimization*', (CRC Press, 2014

Q5

9 Appendix

The variable vectors are

$$\boldsymbol{X} = [\Delta \boldsymbol{P}\ \Delta \boldsymbol{Q}\ \Delta \tilde{\boldsymbol{\delta}}]^{\mathrm{T}}, \quad \Delta \boldsymbol{P} = [\Delta P_1 \cdots \Delta P_n],$$
$$\Delta \boldsymbol{Q} = [\Delta Q_1 \cdots \Delta Q_n], \quad \Delta \tilde{\boldsymbol{\delta}} = \left[\Delta \tilde{\delta}_1 \cdots \Delta \tilde{\delta}_n\right].$$

The system matrix $\boldsymbol{A}$ is written as

$$\boldsymbol{A} = \begin{bmatrix} \boldsymbol{A}_{11} & \boldsymbol{0} & \boldsymbol{A}_{13} \\ \boldsymbol{A}_{21} & \boldsymbol{A}_{22} & \boldsymbol{A}_{23} \\ \boldsymbol{A}_{31} & \boldsymbol{A}_{32} & \boldsymbol{0} \end{bmatrix} \tag{32}$$

where

$$\boldsymbol{A}_{11} = \omega_{\mathrm{c}} \begin{bmatrix} \left(\frac{\partial p_1}{\partial V_1} a_1 - 1\right) & \cdots & \frac{\partial p_1}{\partial V_n} a_n \\ \vdots & \ddots & \vdots \\ \frac{\partial p_n}{\partial V_1} a_1 & \cdots & \left(\frac{\partial p_n}{\partial V_n} a_n - 1\right) \end{bmatrix};$$

$$\boldsymbol{A}_{13} = \omega_{\mathrm{c}} \begin{bmatrix} \frac{\partial p_1}{\partial \tilde{\delta}_1} & \cdots & \frac{\partial p_1}{\partial \tilde{\delta}_n} \\ \vdots & \ddots & \vdots \\ \frac{\partial p_n}{\partial \tilde{\delta}_1} & \cdots & \frac{\partial p_n}{\partial \tilde{\delta}_n} \end{bmatrix};$$

$$\boldsymbol{A}_{21} = \omega_{\mathrm{c}} \begin{bmatrix} \frac{\partial q_1}{\partial V_1} a_1 & \cdots & \frac{\partial q_1}{\partial V_n} a_n \\ \vdots & \ddots & \vdots \\ \frac{\partial q_n}{\partial V_1} a_1 & \cdots & \frac{\partial q_n}{\partial V_n} a_n \end{bmatrix};$$

$$\boldsymbol{A}_{22} = -\omega_{\mathrm{c}} \boldsymbol{I};$$

$$\boldsymbol{I} = \mathrm{diag}[1 \cdots 1]_{n \times n};$$

$$\boldsymbol{A}_{23} = \omega_{\mathrm{c}} \begin{bmatrix} \frac{\partial q_1}{\partial \tilde{\delta}_i} & \cdots & \frac{\partial q_1}{\partial \tilde{\delta}_n} \\ \vdots & \ddots & \vdots \\ \frac{\partial q_n}{\partial \tilde{\delta}_1} & \cdots & \frac{\partial q_n}{\partial \tilde{\delta}_n} \end{bmatrix};$$

$$\boldsymbol{A}_{31} = -2\pi m \begin{bmatrix} \mathrm{sgn}(Q_1^o) \sin \varphi_1^o \frac{\partial \varphi_1}{\partial P_1} & & \\ & \ddots & \\ & & \mathrm{sgn}(Q_n^o) \sin \varphi_n^o \frac{\partial \varphi_n}{\partial P_n} \end{bmatrix};$$

$$\boldsymbol{A}_{32} = -2\pi m \begin{bmatrix} \mathrm{sgn}(Q_1^o) \sin \varphi_1^o \frac{\partial \varphi_1}{\partial Q_1} & & \\ & \ddots & \\ & & \mathrm{sgn}(Q_n^o) \sin \varphi_n^o \frac{\partial \varphi_n}{\partial Q_n} \end{bmatrix}.$$